JOURNAL OF MATERIALS SCIENCE 31 (1996) 5045–5049

The effect of crystallization of the grain-boundary phase on ambient temperature fatigue short-crack growth behaviour in Y–α′-β′-Sialon

GUO-DONG ZHAN, JIAN-LIN SHI, DAN-YU JIANG, FENG-YING WU, TING-RONG LAI, and TUNG-SHENG YEN
The State Key Laboratory of High Performance Ceramics and Superfine Microstructure, Shanghai Institute of Ceramics, Chinese Academy of Sciences, Shanghai 200050, People's Republic of China

The cyclic fatigue short-crack growth behaviour of Y–α′-β′-Sialons with both crystallized and amorphous grain-boundary phases, were investigated to determine whether crystallization of grain boundaries affected crack-growth behaviour under cyclic and monotonic loads. Micromechanisms for fatigue-crack growth in Y–α′-β′-Sialon were examined by scanning electron microscopy and high-resolution electron microscopy. These results show that the wear debris on the fatigue fracture surfaces gave evidence of a frictional wear crack-growth mechanism. Comparison of fatigue short-crack growth rates for Sialon of crystallized grain-boundary phases with that for the amorphous grain-boundary phases indicated that crystallization of grain-boundary phases does not appear to affect cyclic fatigue growth behaviour, similar to long-crack growth behaviour. The similarity of fatigue short-crack growth behaviour in both the crystallized and amorphous grain boundaries sialons is rationalized in terms of the thin residual amorphous grain-boundary regions.

1. Introduction

Recently, extensive studies have concentrated on improving the high-temperature performance of silicon nitride-based ceramics of devitrification of the original amorphous grain-boundary phases to form refractory crystalline structures [1–8]. Because the low self-diffusivity of Si_3N_4 does not allow densification by classical solid-state sintering techniques, processing to near-theoretical density by liquid-phase sintering requires the use of sintering aids. During densification, these additives react with the Si_3N_4 particles, and a eutectic liquid is formed. Upon cooling, the liquid phase remains as amorphous and/or crystalline secondary phases at grain boundaries and multi-grain junctions. These secondary phases, in particular the remaining amorphous phase, are known to deteriorate greatly the high-temperature mechanical properties [2]. One method of improving high-temperature properties is to increase the softening point of the amorphous phases. However, the resulting strength of the ceramics at high temperatures is still far below their room-temperature strength. Another method of improving the high-temperature properties is to promote crystallization of the amorphous phases, in order to eliminate the softening point entirely [3]. Of concern, however, is whether crystallization of grain-boundary phases affects room-temperature crack-growth behaviour under both monotonic and cyclic loads, given the key role of the grain-boundary phase on the micromechanisms of crack growth. Cornelissen *et al.* [8] have investigated the cyclic fatigue "long"-crack growth and fracture toughness of silicon nitride ceramics sintered with selected rare-earth oxides. These results indicated that crystallization of constituent grain-boundary phases to improve high-temperature properties does not appear to degrade room-temperature toughness and fatigue-crack growth resistance. However, the effect of crystallization of the grain-boundary phase on ambient temperature "short" fatigue crack-growth behaviour, to our knowledge, has not been made for this class of material. The principal interest in the present study was the effect of crystallization of the grain-boundary phase in Y-α′-β′-Sialon on room-temperature Vickers' indentation fatigue short-crack growth behaviour.

2. Experimental procedure

2.1. Materials

The starting powders used were Si_3N_4 (laboratory made, N > 38 wt %, O ≃ 1.5 wt %, α-phase > 90 %), AlN (laboratory made, N > 32.5 wt %, O ≃ 1.5 wt %), Al_3O_2 (> 99.95 wt%), Y_2O_3 (> 99.9 wt %). The mixtures of powders were milled in absolute alcohol for 24 h in an alumina jar, using sintered silicon nitride grinding media. After the powder mixtures were dried,

0022–2461

they were die-pressed into bars under 20 MPa and then isostically pressed under a pressure of 250 MPa. Pressed compacts were placed in covered graphite crucible with a protective powder bed of 90 wt % Si_3N_4 + 10 wt % BN, and then sintered at 1950 °C under 1.5 atm nitrogen pressure for 2 h in a gas-pressure sintering furnace. Some of the samples were heat treated for 24 h in 1250 °C so that the amorphous grain-boundary phase could crystallize. Flexural strength was measured in four-point bending in air at room temperature (650 MPa) and fracture toughness measurements were performed on the polished surfaces of the fatigue specimens using indentation techniques (8.5 MPa $m^{1/2}$). No change in mechanical properties after heat treatment was found.

2.2. Microstructural observations

Phase analysis was done by X-ray diffractometry (XRD) using a Rigaku model RAX-10 rotating anode set-up. Microstructural observations were investigated under high-resolution electron microscopy (HREM), a Jeol 200CX equipped with a top-entry double-tilt goniometer. To prepare the samples for HREM, 0.5 mm thin slices were cut by a high-speed diamond saw from the sintered body. One side of each slice was ground and polished to a mirror surface at first, then the other side was ground and polished down to about 100 μm, and finally carefully polished to about 30 μm. The resultant film was then ion-thinned with an argon dual-beam to perforation. In order to avoid surface charging under the high-voltage electron beam, all samples were coated with a thin evaporated carbon film before observation under the electron microscope.

2.3. Fatigue testing

Bar specimens, 40 mm × 4 mm × 3 mm, were machined from the as-received plate and polished to 1 μm diamond surface finish. Initial surface cracks were introduced on the inner span of the tensile side of the specimen, using a Vicker's diamond indentor at load of 98 N. The initial cracks were approximately semi-circular in shape ($c/a = 0.97$) and about 200 μm long. These indents were carefully aligned so that corner cracks emanating from the indents were all parallel or perpendicular to the long axis of the specimen.

A four-point bending configuration with an inner span of 10 mm and an outer span of 30 mm was used in this study. Cyclic bending fatigue tests were conducted using a commercial servohydraulic machine operated under load control, with a sinusoidal wave form at a frequency of 5 Hz and load ratio, R (minimum/maximum loads) of 0.1. The surface crack length was measured by a travelling microscope at a magnification of x120. Following completion of the fatigue-crack growth tests, the fracture surfaces and crack profiles were examined in a scanning electron microscope (SEM). Both fatigue and monotonic fracture regions of fracture surfaces were examined to provide some indication of the micromechanism of crack advance.

2.4. Data processing

Fatigue-crack growth rates were determined over the range 10^{-10}–10^{-6} m cycle^{-1} from crack length versus number of cycles curves. Far-field stress intensity factors were computed from linear-elastic solutions [5] in terms of crack depth, a, half crack length, c, specimen thickness and width, b and t, geometric factors, ϕ and Q, and remote bending stress, σ

$$K_{appa} = H\sigma(\pi a/Q)^{1/2} f(a/c, a/t, a/b, \phi) \quad (1)$$

where H is the bending multiplier and f is a geometric function. To consider the effect of residual stress induced by indentation, an additional stress intensity factor, K_r from the residual crack-opening stress was calculated in terms of indentation load, P, and the half crack length, c, by [6]

$$K_r = \chi P c^{-3/2} \quad (2)$$

where the prefactor χ is a material constant, depending on elastic modulus and microhardness. The total (effective) stress intensity factor at crack tip is therefore given by the summation of Equations 1 and 2. The slope of a straight line fitted to the log–log plots of growth rate (da/dN) versus the total stress intensity factor range, ΔK, data allowed determination of the exponent m and C in the Paris power-law relationship [1]

$$da/dN = C(\Delta K)^m \quad (3)$$

3. Results and discussion

3.1. General microstructural features

The X-ray diffraction analysis of the sample indicates the phase compositions of the sample after gas-pressure sintering contain α′-Sialon (37 vol %) and β′-Sialon (63 vol %) as the two major crystalline phases with some grain-boundary phases. Fig. 1 shows a scanning electron micrograph of the multiphase Sialon. It can be seen that α′-Sialon grains are generally equiaxed in shape; β′-Sialon grains show a whisker-like morphology and the aspect ratio can reach 8–10.

Fig. 2 shows a high-resolution image of a grain boundary between α′-Sialon and α′-Sialon. One of the α′-Sialon grains was viewed along the (1 0 3) plane, while another α′-Sialon grain was viewed along the (3 2 5) plane. There are some glassy grain boundaries between them. The width of the grain boundary is rather thick. For comparison, the structure of the post-heat-treated Sialon is shown in Fig. 3. From this figure, a very small glassy phase between α′-Sialon and α′-Sialon after heat treatment can be seen. Also, Fig. 4 shows a high-resolution image of triple grain boundaries between α′-Sialon, α′-Sialon and a crystallized grain boundary. It shows some residual amorphous phases between triple points and Sialon grains still exist even though heat treatment has been carried out.

3.2. Crack-growth behaviour

The graph in Fig. 5 shows the relationship between the crack-growth rate, da/dN, and the total stress intensity range, ΔK, for Y–α′-β′-Sialon with

Figure 1 A scanning electron micrograph of the multiphase Sialon showing equiaxed α′-Sialon grains and whisker-like β′-Sialon grains.

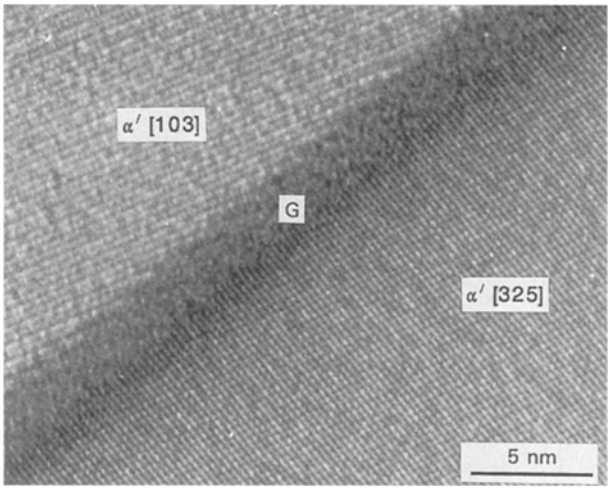

Figure 2 A high-resolution image of a grain boundary between α′-Sialon viewed along the (1 0 3) plane and α′-Sialon viewed along the (3 2 5) plane showing glassy grain boundary, G, between them.

amorphous phases under a cyclic frequency of 5 Hz and load ratio of 0.1 compared to that for crystallized grain boundary. Curves of this form were obtained from five to nine specimens tested. Fatigue-crack growth curves for more ductile metallic materials often exhibit three distinct regions, i.e. near-threshold, mid-, and high-growth rate regimes, but no such regions could be distinguished for the present study. Linear fits to the log–log plots of all data yielded 28 and 29 for the exponent m in Paris' power law for Sialons with the crystallized and amorphous phases, respectively. This is consistent with long-crack results

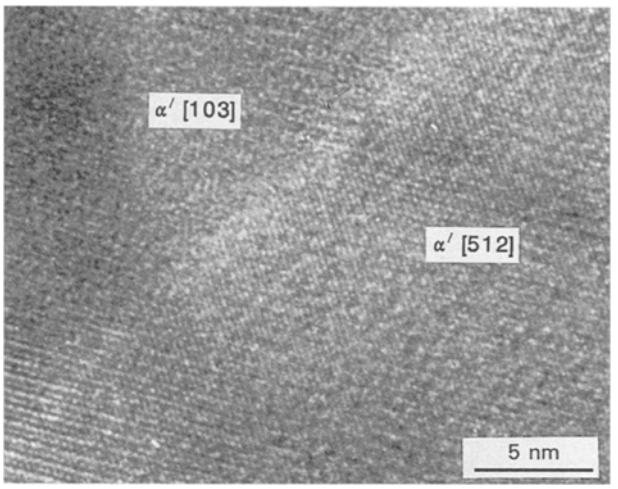

Figure 3 A high-resolution image of a grain boundary between α′-Sialon viewed along the (1 0 3) plane and α′-Sialon viewed along the (5 1 2) plane after heat treatment showing a very small glassy grain boundary between them.

with very higher Paris power exponent, m [1–4]. As can also been seen from this figure, the room-temperature fatigue resistance of Sialon with crystallized grain-boundary phases is comparable to that of Sialon with amorphous grain-boundary phases, because the Paris power exponent in both cases is almost equal. This similarity in crack-growth behaviour may be due to thin residual amorphous grain-boundary regions at the interfaces between adjacent Sialon grains and between the crystallized grain-boundary phases and matrix grains (Fig. 3). Because these interfaces are the preferred stable and fast fracture paths, the immediate crack-tip environment, and more importantly, the formation of a grain-bridging zone, may not be affected significantly by crystallization of grain-boundary phases at triple points [7].

3.3. Crack-growth mechanisms

The scanning electron micrographs in Fig. 6 show the fatigue-crack growth and monotonic fracture surfaces of Sialon with crystallized grain-boundary phases. Region A is the fatigue-crack growth region with intergranular fracture of α′-Sialon grains and Region B is the monotonic fracture region with transgranular fracture of α′-Sialon grains. However, the fracture of β′-Sialon grains is primarily intergranular in both cases. Whisker-like β′-Sialon grains and evidence of pull-out of β′-Sialon grains are clearly visible. Note also that the resulting fatigue fracture surfaces revealed extensive wear debris generated during repeated opening and closing of the crack. The debris was identified as the grain-boundary phase produced at triple points after crystallization [8]. Such wear debris provides evidence for a frictional wear mechanism for fatigue-crack growth [4]. The marked increase in debris apparently results from crystallization of the grain-boundary triple points which produces a phase more prone to microcracking and wear degradation compared to the amorphous grain-boundary phase [4, 8]. Also, observations of crack propagation reveal

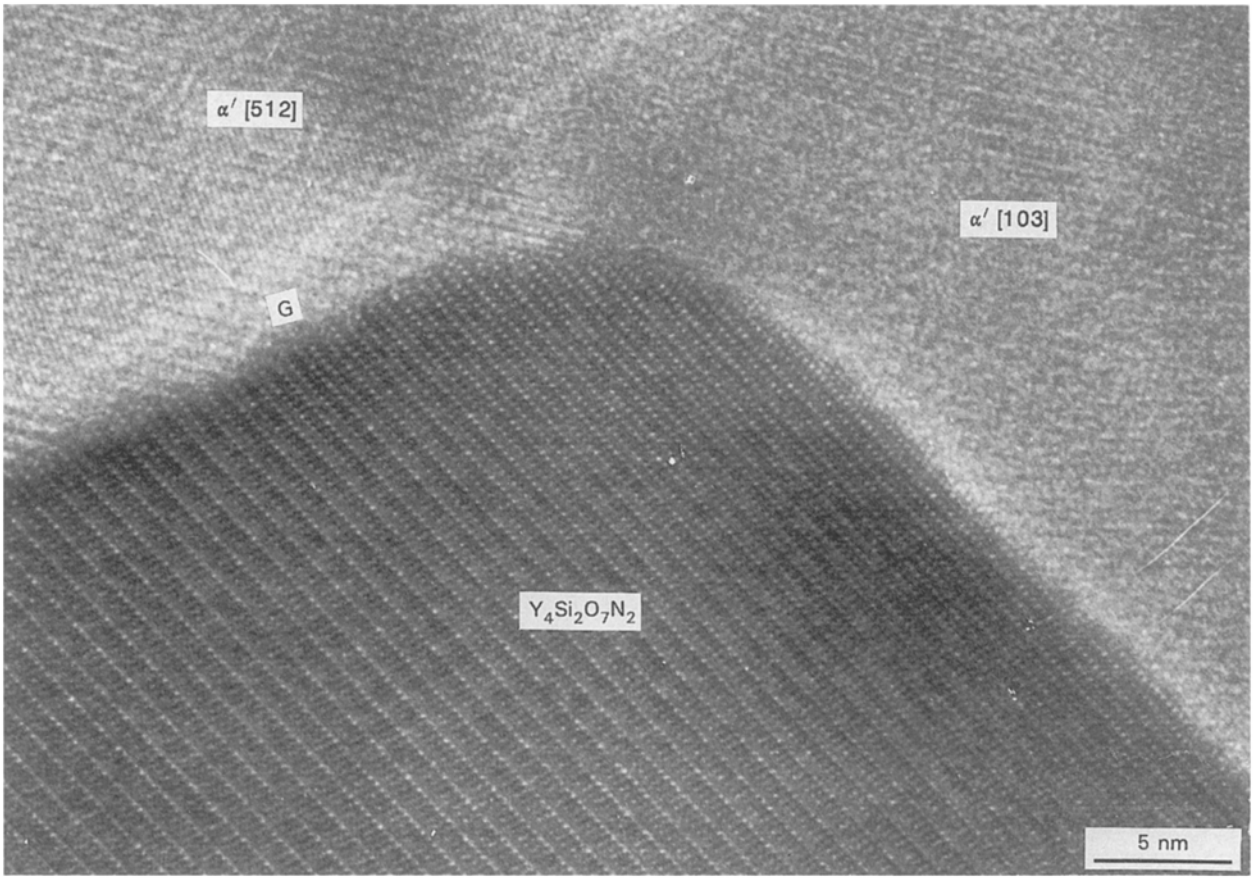

Figure 4 A high-resolution image of triple grain boundaries between α′-Sialon, α′-Sialon and crystallized grain-boundary phase ($Y_4Si_2O_7N_2$) after heat treatment showing some residual amorphous phases between triple points and Sialon grains.

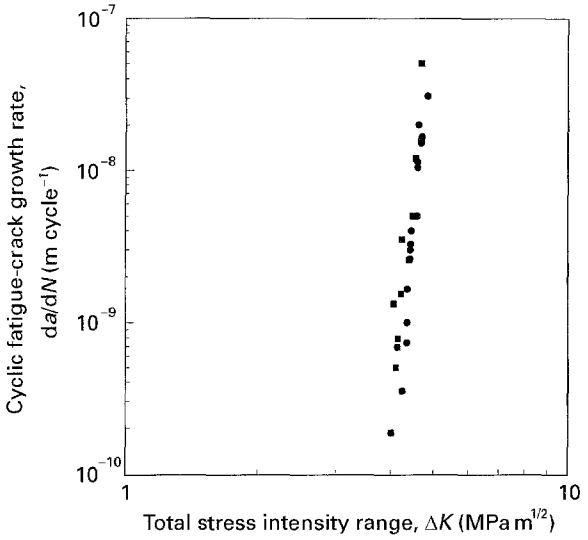

Figure 5 The relationship between the crack-growth rate, da/dN, and the total stress intensity range, ΔK for Y–α′-β′-Sialon with (■) crystallized and (●) amorphous grain-boundary phases under a cyclic frequency of 5 Hz and load ratio of 0.1. For amorphous phase, $da/dN = 3.96 \times 10^{-28}$ $(\Delta K)^{29}$; for crystallized phase, $da/dN = 3.56 \times 10^{-27}$ $(\Delta K)^{28}$, α′; β′ = 37; 63 vol%.

the occurrence of whisker-like β′-Sialon bridging behind the crack tip (Fig. 7). Owing to the extremely limited crack-tip plasticity in Si_3N_4-based ceramics, other non-linear elastic processes, such as frictional sliding of crack-wake bridges behind the crack tip, have been identified as sources for fatigue degradation

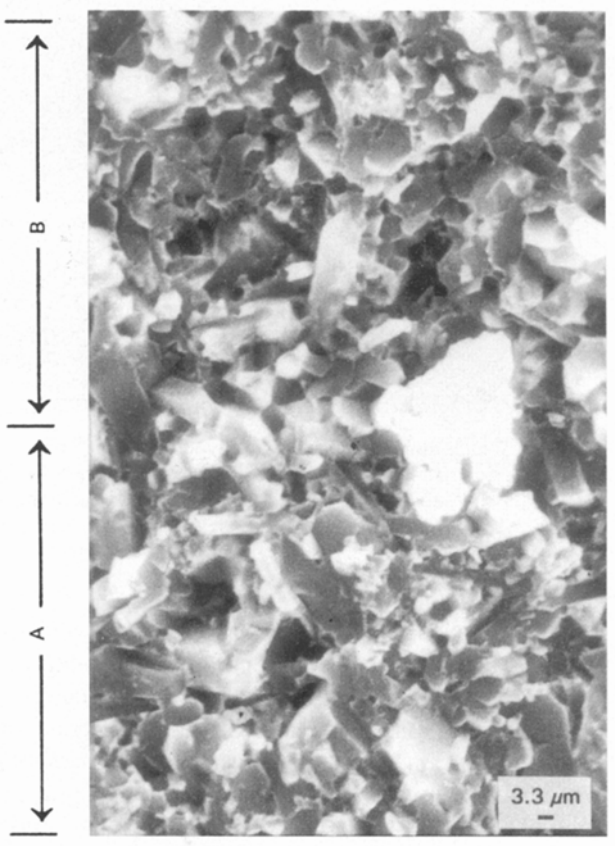

Figure 6 Scanning electron micrograph of the fatigue region A and fast fracture region B of Sialon with crystallized grain-boundary phases. Note that a marked increase of wear debris was apparent on the fatigue region.

Figure 7 Scanning electron micrograph of the fatigue-crack propagation showing the occurrence of whisker-like β′-Sialon bridging behind the crack tip.

[7, 8]. In particular, the repetitive opening and closing of the crack results in a decrease in the toughening capacity of the bridging zone by reducing the grain-bridging stress, i.e. accumulated damage and reduced frictional sliding resistance from progressive wear at the grain/matrix interface causes a significantly reduced frictional pull-out stress under cyclic compared to monotonic loading [7]. In Y–α′-β′-Sialon made of equiaxed α′-Sialon grains and whisker-like β′-Sialon, bridging of crack faces by whisker-like β′-Sialon grains can shield the crack tip from the applied stress intensity and reduce the stress intensity experienced by the crack tip from the applied value to an effective one.

4. Conclusions

Based on a study of cyclic fatigue-crack growth behaviour from Vickers' indentation in Y–α′-β′-Sialon with both crystallized and amorphous grain-boundary phases, the following conclusions can be drawn.

1. Fatigue-crack growth rates exhibit a power-law dependency on the effective stress intensity factor of the crack tip, with a high crack-growth exponent, similar to behaviour in other ceramic materials. Crack-growth rates for Sialon with crystallized grain-boundary phases were found to be comparable to that of Sialon with amorphous grain-boundary phases. The crystallization of the grain-boundary phase does not appear to affect ambient temperature fatigue short-crack growth behaviour.

2. Scanning electron microscopy of fatigue and fast fracture surfaces showed that the fatigue-crack growth region is intergranular fracture of α′-Sialon grains and the monotonic fracture region is transgranular fracture of α′-Sialon grains. However, the fracture of β′-Sialon grains is intergranular in both cases. Debris indicative of a frictional wear fatigue short-crack growth mechanism was also observed. Micromechanisms of cyclic fatigue-crack growth are reasoned to be the wear degradation of frictional whisker-like β′-Sialon grain bridges.

Acknowledgement

Guo-Dong Zhan was supported by a project of the Chinese Post-Doctoral Research Foundation.

References

1. A. TSUGE, K. NISHIDA and M. KOMATSU, *J. Am. Ceram. Soc.* **58** (1975) 323.
2. R. O. RITCHIE and R. H. DAUSKARDT, *J. Ceram. Soc. Jpn* **99** (1991) 1047.
3. R. H. DAUSKARDT, M. R. JAMES, J. R. PORTER and R. O. RITCHIE, *J. Am. Ceram. Soc.* **75** (1992) 759.
4. R. H. DAUSKARDT, B. J. DALGLEIGH, D. YAO and R. O. RITCHIE, *J. Mater. Sci.* **28** (1993) 3258.
5. M. YODA, *Int. J. Fract.* **39** (1989) R23.
6. L. EWART and S. SURESH, *J. Mater. Sci. Lett.* **5** (1986) 774.
7. R. H. DAUSKARDT, *Acta Metall. Mater.* **41** (1993) 2765.
8. B. E. CORNELISSEN, R. H. DAUSKARDT, R. O. RITCHIE and G. THOMAS, *ibid.* **42** (1994) 3055.

Received 11 January
and accepted 18 March 1996